



**HAL**  
open science

## Advances in modelling gold nanoparticle radiosensitization using new Geant4-DNA physics models

Elette Engels, Samer Bakr, David Bolst, Dousatsu Sakata, Nan Li, Peter Lazarakis, Stephen McMahon, Vladimir Ivanchenko, Anatoly Rosenfeld, Sébastien Incerti, et al.

### ► To cite this version:

Elette Engels, Samer Bakr, David Bolst, Dousatsu Sakata, Nan Li, et al.. Advances in modelling gold nanoparticle radiosensitization using new Geant4-DNA physics models. *Physics in Medicine and Biology*, 2020, 65, pp.225017. 10.1088/1361-6560/abb7c2 . hal-02988406

**HAL Id: hal-02988406**

**<https://hal.science/hal-02988406>**

Submitted on 9 Nov 2020

**HAL** is a multi-disciplinary open access archive for the deposit and dissemination of scientific research documents, whether they are published or not. The documents may come from teaching and research institutions in France or abroad, or from public or private research centers.

L'archive ouverte pluridisciplinaire **HAL**, est destinée au dépôt et à la diffusion de documents scientifiques de niveau recherche, publiés ou non, émanant des établissements d'enseignement et de recherche français ou étrangers, des laboratoires publics ou privés.

# Advances in modelling gold nanoparticle radiosensitization using new Geant4-DNA physics models

Elette Engels<sup>1,2\*</sup>, Samer Bakr<sup>1</sup>, David Bolst<sup>1</sup>, Dousatsu Sakata<sup>1</sup>, Nan Li<sup>1,2</sup>, Peter Lazarakis<sup>1</sup>, Stephen J. McMahon<sup>3</sup>, Vladimir Ivanchenko<sup>4,5</sup>, Anatoly B. Rosenfeld<sup>1,2</sup>, Sébastien Incerti<sup>6,7</sup>, Ioanna Kyriakou<sup>8</sup>, Dimitris Emfietzoglou<sup>8</sup>, Michael L. F. Lerch<sup>1,2</sup>, Moeava Tehei<sup>1,2</sup>, Stéphanie Corde<sup>1,2,9</sup>, Susanna Guatelli<sup>1,2</sup>

<sup>1</sup> Centre for Medical Radiation Physics, University of Wollongong, NSW, Australia.

<sup>2</sup> Illawarra Health and Medical Research Institute, University of Wollongong, NSW, Australia.

<sup>3</sup> Centre for Cancer Research and Cell Biology, Queens University, Belfast, Northern Ireland BT7 1NN

<sup>4</sup> Tomsk State University, Tomsk, Russian Federation.

<sup>5</sup> CERN, Espl. des Particules 1, 1211 Meyrin, Switzerland

<sup>6</sup> CNRS, UMR5797, Centre d'Etudes Nucléaires Bordeaux Gradignan (CENBG), Chemin du Solarium, Gradignan, France

<sup>7</sup> Université de Bordeaux, Centre d'Etudes Nucléaires Bordeaux Gradignan (CENBG), Chemin du Solarium, Gradignan, France

<sup>8</sup> Medical Physics Laboratory, Dept. of Medicine, University of Ioannina, 45110, Ioannina, Greece

<sup>9</sup> Prince of Wales Hospital, Randwick, New South Wales, Australia

\*E-mail: ee215@uowmail.edu.au

## Abstract

Gold nanoparticles have demonstrated significant radiosensitization of cancer treatment with X-ray radiotherapy. To understand the mechanisms at the basis of nanoparticle radiosensitization, Monte Carlo simulations are used to investigate the dose enhancement, given a certain nanoparticle concentration and distribution in the biological medium. Earlier studies have ordinarily used condensed history physics models to predict nanoscale dose enhancement with nanoparticles. This study uses Geant4-DNA complemented with novel track structure physics models to accurately describe electron interactions in gold and to calculate the dose surrounding gold nanoparticle structures at nanoscale level. The computed dose *in silico* due to a clinical kilovoltage beam and the presence of gold nanoparticles was related to *in vitro* brain cancer cell survival using the Local Effect Model. The comparison of the simulation results with radiobiological experimental measurements shows that Geant4-DNA and Local Effect Model can be used to predict cell survival *in silico* in the case of X-ray kilovoltage beams.

Keywords: Geant4, Geant4-DNA, Gold Nanoparticles, Dose Enhancement, Cell Survival, Local Effect Model

---

## 1. Introduction

High atomic number ( $Z$ ) nanoparticles (NPs), such as gold, platinum and ceramic metal oxide particles are sub-cellular in size and are ideally suited to internalize within cells (Jain et al 2012, Engels et al 2017, Engels et al 2018, Chithrani et al 2009). When exposed to X-rays used in radiotherapy, NPs enhance local radiation doses and increase cancerous cell destruction (Her et al 2017). This is due to an excess of low energy electrons produced from the NPs, which deposit

energy locally in the surrounding biological medium (Jain et al 2012).

With inert properties and high  $Z$  of 79, gold NPs (GNPs) are among the most researched candidates for NP-enhanced cancer treatment using methods such as Monte Carlo simulations (Tran et al 2016, McKinnon et al 2016, Zygmanski and Sajo 2016, Liu et al 2019), and both *in vitro* (McDonald et al 2018, Lin et al 2014) and *in vivo* studies (Hainfeld et al 2008, 2013). The enhanced photoelectron production, emission of low energy Auger electrons and fluorescence X-rays associated with the high- $Z$  of gold cause

significant localized damage to cancer cells, particularly in kilovoltage (kV) radiation fields (Lin et al 2014, Mesbahi 2010). Currently, kV radiotherapy is used to treat skin cancer (Kin and Kim 2017, 2018), but could be used to treat brain and central nervous system cancers (CNS), (Grotzer et al 2015, Engels et al 2016, Joh et al 2013, Engels et al 2020).

Where normal tissue sparing remains a concern with standalone radiation treatments, GNPs offer a means to better target cancerous cells, maintaining tumor control, while reducing the normal tissue radiation dose (Mesbahi 2010). Optimal energies for dose enhancement effects with GNPs is estimated to be 60–90 keV using monochromatic beams due to the comparatively smaller X-ray absorption of tissues (or water) at these energies (Boudou et al 2005).

### 1.1 Monte Carlo simulation and GNP-enhanced radiotherapy

Monte Carlo (MC) simulations describe particle transport in matter and interactions, and are widely used to investigate the energy deposition around GNPs in the biological medium when irradiated by a radiotherapeutic field. Simulations determine the effect of varying the size, distribution and shape of the GNPs (Jones et al 2010, Cho 2005).

The physics models, included in the “general purpose” MC codes such as EGS (Nelson et al 1985), PENELOPE (Baró et al 1995), Geant4 (Agostinelli et al 2003), and MCNP (X-5 Monte Carlo Team, 2005) adopt a condensed history (CH) approach, where a large number of collision processes are grouped together (“condensed”), producing an artificial mean free path called a “step”. This approach has made MC simulations a highly useful investigation tool, but inherently inadequate to describe detailed particle interactions at nanometer scale and low energy (< keV).

Specialized MC codes, such as PTra (Grosswendt 2002) PARTRAC (Friedland et al 2011), KURBUC (Nikjoo et al 2016), NOREC (Grosswendt 2002), and TRAX (Semenenko et al 2003) usually known as “track structure codes” (TS codes), have been developed to calculate the energy deposition at nanometer scale, modelling particle tracks according to each physics process occurring, typically in gaseous medium or liquid water, to approximate biological systems (Nikjoo et al 2016).

The Geant4 electromagnetic physics classes adopt the CH approach and contain models addressed to medical physics applications (Arce et al 2020). One is based on the Livermore evaluated data library (Cirrone et al 2010) with a recommended low-energy limit of 250 eV (Cullen et al 1991, 1997, Perkins et al 1991). The second one is based on the Penelope MC code, valid down to approximately 100 eV (Fernandez-Varea et al 2012, Lazarakis et al 2018, Kyriakou et al 2019).

Geant4 is the only general-purpose radiation transport MC code which offers TS physics models to describe particle

interactions in liquid water at nanometer level, through the Geant4-DNA Package (G4DNA), (Incerti et al 2010, 2010, 2018, Bernal et al 2015). This package currently provides a complete set of models describing process by process the electromagnetic interactions of particles (including electrons, protons, alpha particles and ions) with liquid water (Bernal et al 2015).

Sakata *et al* (2016) developed the first TS-based physics models within G4DNA capable of describing electron interactions in GNPs (Sakata et al 2016, 2018). Such models have been refined in a second iteration, where the Energy Loss Function formalism has been adopted to describe the ionization and excitation processes in gold down to ~10 eV (Sakata et al 2019). The new gold models adopt the ELSEPA code to calculate elastic scattering cross-section (Sakata et al 2016).

### 1.2 Modelling cell survival

Translation from Monte Carlo simulations to *in vitro* experimental results is still sought after, particularly concerning the nanoscale dose inhomogeneity produced by GNPs. The linear quadratic model (LQM) is based on the linear quadratic nature of the cell survival curve, (McMahon 2019, Lechtman et al 2013). The LQM relates the average dose,  $D$ , delivered to the cell population with X-rays, to the cell surviving fraction,  $S_X$ , according to Equation 1.

$$S_X = \exp(-(\alpha D + \beta D^2)) \quad (1)$$

The parameters  $\alpha$  and  $\beta$  relate  $D$  to  $S_X$  and can be evaluated experimentally *in vitro*. The LQM, in its simplicity, is ideally suited to describe the effect of averaged and uniform radiation field doses on cell survival. Due to this, the LQM is not well-suited to spatially fractionated or non-uniform dose fields such as microbeam radiation therapy (Grotzer et al 2015) and particle therapy (Tran et al 2016, Scholtz and Kraft 1994). This has led to the development of other radiobiological models including the Local Effect Model (LEM), (Scholz and Kraft 1994, 1996, 2004).

The LEM, described in Equations 2 and 3, is a more sophisticated approach to dose non-uniformity than the LQM and was originally developed to determine the radiobiological effectiveness of heavy ion radiation field for hadron therapy applications (Scholz and Kraft 1994). LEM relates energy depositions on the nanoscale to the cell survival  $S$ , determined from *in vitro* experiments.  $S$  can be expressed as function of the number of lethal events,  $N$ , following Poisson statistics, equivalent to Equation 2.

$$S = \exp(-N) \quad (2)$$

$N$  is calculated by means of Equation 3 where the local dose in the biological medium,  $D(x,y,z)$ , due to the incident X-ray

field is used to compute a spatially dependent  $S(D(x,y,z))$ , obtained using Equation 1, which is evaluated at nanoscale volumes ( $dV$ ) within a sensitive volume,  $V_s$ .

$$N = - \int_{V_s} \frac{\ln(S(D(x,y,z)))}{V_s} dV \quad (3)$$

The average number of lethal events due to a non-uniform radiation field, such as the one obtained with NPs internalized in the cell ( $N_{NP}$ ), can also be evaluated using this approach. Implementation of the LEM for this purpose is described further in the method for our study.

Many correlations to *in vitro* studies with GNPs have been made using LEM (McMahon et al 2011, 2019, Lechtman et al 2013, Ferrero et al 2017), however, this is the first study to investigate the impact of new specialized G4DNA gold physics models (Sakata et al 2016, 2018) in GNP radio - enhancement and how this is related to cell survival *in vitro* for a more realistic GNP distribution. This work calculates the dose enhancement on the nanoscale with a single GNP and a simplistic model of the clustering GNPs around the cell nucleus. G4DNA, with the novel specialized gold TS physics models was compared to the case with the CH Livermore Package to describe particle interactions in the medium. The cell surviving fraction with GNPs was then calculated *in silico* by applying the LEM to 9L gliosarcoma cancer cells irradiated with kV X-rays. Direct correlation was made between the computed cancer cell survival and the *in vitro* results with GNPs.

## 2. Method

### 2.1 Cell experiment design

Cell experiments were carried out with 9L gliosarcoma (9LGS), rat glioma cells derived from an N-nitroso-N-methylurea (NMU)-induced tumor and were purchased from the European Collection of Cell Cultures (ECACC). Cell cultures were maintained at 37 °C and 5% (v/v) CO<sub>2</sub> in a T75 cm<sup>2</sup> tissue culture flask containing complete-DMEM (Dulbecco's Modified Eagle Medium, Gibco®, Life Sciences), supplemented with 10% (v/v) FBS (Fetal Bovine Serum, Invitrogen) and 1% (v/v) PS (penicillin/streptomycin, Gibco®, Life Sciences).

GNPs with a diameter of 15 nm are studied in many radiosensitization studies (Her et al 2017, McQuaid et al 2016). They are commonly used *in vitro* and *in vivo* experiments as they have low toxicity (Bobyk et al 2013), and show more lingering internalization and efficient localization at tumor site through the vasculature supply (Domey et al 2015). AuroVist™ 15 nm diameter NPs are commercially available for preclinical use (Nanoprobe Inc., NY). To prepare the GNPs, a portion of the original 200 mg/mL GNP

stock was diluted in phosphate buffered saline (PBS, Gibco®) to a final concentration of 10 mg/mL.

#### 2.1.1 Cell Imaging for Simulation Set up

Confocal imaging was performed to determine the distribution of GNPs in 9LGS, adapting a similar method outlined by Kim *et al.* (2015).

9LGS cells were incubated with or without GNPs in an ibidi®  $\mu$ -slide, 8 well, chambered coverslip (ibidi GmbH, Lochhamer Schlag 11, 82166 Gräfelfing). GNPs were added to 9LGS cell medium 24 hours before imaging, at a final concentration of 500  $\mu$ g/mL. Images were acquired with a Leica TCS SP5 confocal microscope (Leica Microsystems Pty Ltd, Macquarie Park, 2113 Australia). After 24 hour incubation, the  $\mu$ -slide was placed directly in the confocal microscope (without washing) on a movable stage and a 40x oil immersion lens used to image cells once immersion oil was applied to the slide. An argon laser with wavelength 488 nm was used to expose the cells and GNPs, in order to produce fluorescence or light scatter from the sample. Light was detected using a photomultiplier tube in the range of 510 – 600 nm. Bright field images were also collected. Images were obtained at multiple depths within the cell.

Figure 1 shows a confocal microscopic image of GNPs inside the 9LGS cells, with pixel size of 0.48  $\mu$ m by 0.48  $\mu$ m. The green light scatter indicates the presence of GNPs by exploiting the surface plasmon resonance of gold above 10 nm (Kim et al 2015) and shows that the GNPs tend to congregate around the cell nucleus of the 9LGS. This motivated the use of a simplistic geometrical model of the GNP configuration for the evaluation of the LEM.

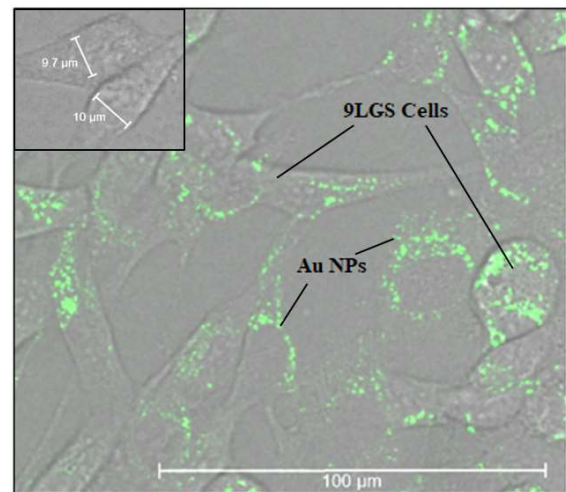


**Figure 1.** Confocal microscopy of GNPs (shown in green) incubated in 9LGS for 24 hours at a concentration of 500  $\mu$ g/mL. Insert (top-left), shows image of 9LGS cells without argon laser illumination. Dimensions of cell nuclei are shown.

When using bright field (BF) imaging alone (no laser, as shown in Figure 1, top-left), there is no visible evidence of GNPs. The accumulations of GNPs therefore are of a size much less than the BF visible resolution of  $0.48\ \mu\text{m}$ , and only appear present with laser light. These experimental findings have prompted the use of a GNP upper size limit of  $100\ \text{nm}$  diameter in the simulation study to mimic the order of magnitude of the largest possible GNP clusters, as well as the original single GNPs that are  $15\ \text{nm}$  diameter.

In biological experiments multiple GNPs and GNP clusters often develop into larger structures which affect the dose enhancement of the GNPs to the cell (McKinnon et al 2016, Liu et al 2019). For the LEM method, the GNP-shell geometry resembling the realistic GNP distribution was therefore considered by recording the positions of the GNPs over the entire volume of the 9LGS cell. On average, a shell-like distribution was seen, as shown in Figure 1, which was estimated in 3 dimensions to be 1 GNP thick throughout the shell. It was also found that the GNPs were less likely to be on the top of the nucleus or on the bottom against the flask. Therefore, a GNP shell distribution was modelled  $2\ \mu\text{m}$  from the top of the 9LGS nucleus,  $6\ \mu\text{m}$  deep, and surrounding the 9LGS nucleus of  $10\ \mu\text{m}$  diameter (see Figure 4).

### 2.1.2 Cell Irradiation

24 hrs prior to irradiation,  $500\ \mu\text{g}/\text{mL}$  GNPs were added to 9LGS cells that were sub-cultured into  $T12.5\text{cm}^2$  flasks (BD Falcon<sup>TM</sup>) containing c-DMEM. The irradiation of 9L cells with and without GNPs was performed at the Prince of Wales Hospital (Randwick, New South Wales, Australia 2031) using a Nucletron Oldelft Therapax DXT 300 Series 3 Orthovoltage X-ray machine (Nucletron B.V., Veenendaal, The Netherlands).  $T12.5\text{cm}^2$  flasks containing a monolayer of 9L cells under  $6\ \text{mm}$  medium were positioned at a distance of  $50\ \text{cm}$  from the X-ray tube. Flasks rested on a  $10\ \text{cm}$  solid water phantom and were surrounded by  $6\ \text{mm}$  of solid water to ensure full particle equilibrium. X-rays were generated at  $150\ \text{kVp}$  with a beam current of  $20\ \text{mA}$  using inherent filtration of  $3\ \text{mm}$  beryllium with additional  $0.35\ \text{mm}$  of copper and  $1.5\ \text{mm}$  of aluminum ( $\text{HVL} = 0.68\ \text{mm Cu}$ ). Cells were irradiated with a dose rate of  $0.754\ \text{Gy}/\text{min}$  for doses ranging from  $1$  to  $8\ \text{Gy}$  at  $6\ \text{mm}$  depth. Figure 2 shows the  $150\ \text{kVp}$  spectra. Following the X-ray irradiation, cells were seeded at low density into  $100\ \text{mm}$  petri dishes containing  $10\ \text{mL}$  of c-DMEM. Each independent flask was seeded in triplicate sets corresponding to each radiation dose including an unirradiated control sets with and without GNPs to determine any toxicity due to GNPs. After 14 doubling times (necessary to obtain an adequate number of colonies), each dish was washed with  $5\ \text{mL}$  PBS (calcium and magnesium positive) and stained with a solution of 25% crystal violet solution (2.3% crystal violet, 0.1% ammonium oxalate, 20% ethyl alcohol, from Sigma-Aldrich®, Australia) and 75% ethanol (v/v).

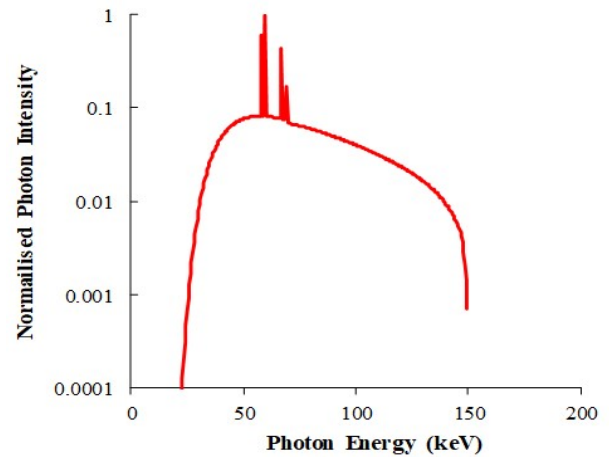


**Figure 2.**  $150\ \text{kVp}$  orthovoltage X-ray spectra (generated using SpekCalc, Poludniowski et al 2009) used to irradiate 9LGS cells experimentally and used in the simulation.

Surviving colonies of 50 cells or more were counted and divided by the original seeding number to determine the plating efficiency (PE). For each treatment group, the PE was averaged, and standard deviation of the mean calculated. The surviving fraction  $S_X$  was evaluated by taking the ratio of the PE of the treated cells and the PE of the non-irradiated control.

## 2.2 Simulation methods

### 2.2.1 Characterization of single GNP dose enhancement

To compare G4DNA TS physics models with the CH Livermore models, a single GNP was simulated using Geant4 10.4 patch01 and placed at  $6\ \text{mm}$  depth in a liquid water phantom with dimensions of  $12 \times 12 \times 12\ \text{mm}^3$  to replicate the setup of the experimental study. A schematic of the simulation geometry is shown in Figure 3.

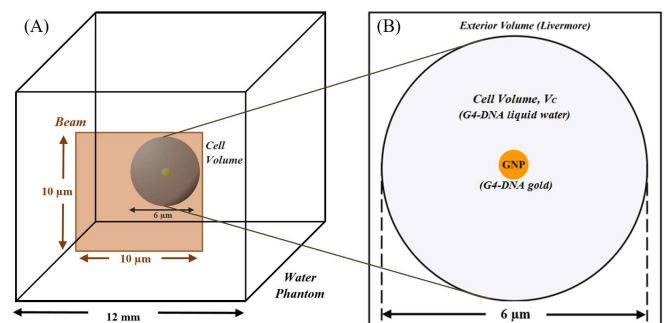


**Figure 3.** Geometry of the Monte Carlo simulation (sizes not to scale). The X-ray beam is incident normally on the water phantom (A). The orange box shows the lateral dimensions of the incident beam. A single GNP is set at  $6\ \text{mm}$  depth in the phantom. The G4DNA is active within  $V_C$  ( $6\ \mu\text{m}$  diameter sphere), with Livermore physics in the surrounding water volume, as shown in the magnified view (B).

The incident radiation field modelled in the Geant4 simulation was the 150 kVp orthovoltage X-ray beam used in the experiment (Figure 2). A maximum of  $10^{11}$  histories were simulated to obtain each set of results. The beam was incident normally to the water phantom with a lateral size of  $10\ \mu\text{m}$ . Two GNP radii were considered; a GNP radius of 7.5 nm, corresponding to the real dimension of individual GNPs, and 50 nm, to mimic a GNP aggregate, as observed with confocal imaging (Figure 1). A cell volume ( $V_C$ ) was added to encompass the GNP with dimensions shown in Figure 3B.

The following situations were considered when modelling the physics processes in the simulation:

1. G4DNA in the GNP (gold material) and  $V_C$  (liquid water material). A cut of 10 eV was adopted. The newly developed G4DNA models specialized for gold targets (described in Sakata et al 2018) were used to model electron interactions in the GNP. The Livermore physics models were used to describe particle interactions in the water phantom surrounding the  $V_C$ , up to a distance of 6 mm, to reduce simulation execution times.
2. Livermore physics models were used throughout all the geometrical set-up (that is within the GNP, within  $V_C$  and in the water phantom surrounding  $V_C$ ).

Atomic de-excitation was also modelled. Auger electrons and fluorescence photons were simulated, including the full relaxation cascade.

The Livermore physics models were adopted for the CH approach because Lazarakis *et al* (2018) and Kyriakou *et al* (2019) showed that such models could begin to approximate G4DNA better than the other available CH approaches of Geant4 when using a 10 eV secondary electron production lower energy limit, while a limit of 250 eV has been recommended by the authors of the Livermore models (Guatelli et al 2007).

The low electron energy (LEE) limit controls the cut of the secondary electron production in the CH models. The LEE limits of 10 eV and 250 eV were investigated in this study of the case of a 50 nm radius GNP radioenhancement.

The simulation calculated the radial absorbed dose distribution from the surface of the GNP per incident photon and the Dose Enhancement Ratio (DER). The DER is the ratio of the absorbed dose with and without the GNP in water.

### 2.2.2 Dose enhancement of a GNP in a partial shell configuration

A GNP shell-like configuration was considered to match experimental observations (Figure 1) and is similar to the distribution previously described in McKinnon *et al.* (2016) and Liu *et al.* (2019). This design was considered as there were some initial discrepancies with LEM using single GNPs (not

shown) that we estimated were due to incorrect extrapolation of realistic GNP geometry in 9LGS.

$V_C$ , originally 3  $\mu\text{m}$  in radius, was increased to 10  $\mu\text{m}$  in radius to encompass the 9LGS cell nucleus which has a radius of 5  $\mu\text{m}$ , based on experimental observations (Figure 1). The beam dimensions were increased to  $24 \times 24\ \mu\text{m}^2$  accordingly.

In this geometrical cell configuration, the cell ‘nucleus’ with radius 5  $\mu\text{m}$ , was partially surrounded with a 15 nm thick GNP shell. The confocal imaging showed that the GNPs were only visible using light scatter from the 20 mW Argon laser, and have sizes smaller than the visible resolution. The GNP shells were sometimes incomplete or had regions of thicker deposits of GNPs. On average, the coverage of the GNPs around the nucleus of 9LGS was approximated to be 1 GNP thick (15 nm) with the top and bottom of the nucleus uncovered by GNPs. This geometry in a simplistic sense mimics the average GNP distribution surrounding the 9LGS nucleus using confocal imaging, and is shown in Figure 4.

Figure 4 represents the geometrical set-up in Geant4, including dimensions of the GNP shell and position of the incident beam. The inner radius of the GNP shell was set equal to 5  $\mu\text{m}$  based on the 9LGS nucleus size in the confocal images. The energy deposited within the cell nucleus was scored as well as 5  $\mu\text{m}$  outside the shell. G4DNA and Livermore physics models were activated for this simulation as described in the next section.

### 2.3 Analysis using LEM-based radiobiological models

To determine the effect of the average dose enhancement due to the GNP shell congregation, a LEM approach was considered which adapts equations 2 and 3. The dose  $D(x,y,z)$  is calculated in terms of radial distance  $r$ , as  $D(r)$ , and ranges from the origin at the center of  $V_C$  to the interior surface of the GNP shell in 1 nm steps ( $\Delta r = 1\ \text{nm}$ ), denoted by the total radius of  $V_C$  ( $R_C$ ).

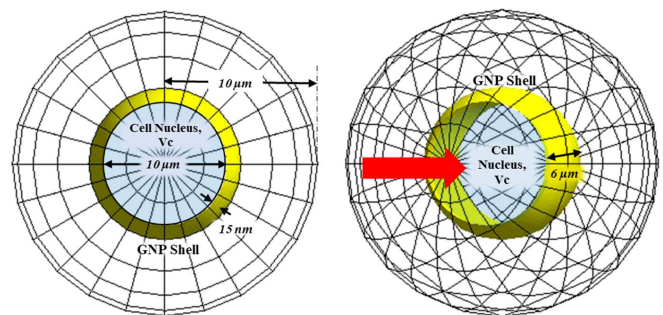


**Figure 4.** The partial GNP shell (yellow) modelled in the Geant4 simulation, shown from a beam view and 30° perspective. The red arrow shows the direction of the incident beam. The 6  $\mu\text{m}$ -wide GNP shell surrounds  $V_C$  and begins at 2  $\mu\text{m}$  depth from the surface of  $V_C$ , and was constructed to surround 60% of the cell as estimated from confocal imaging.

Equation 3 can then be used to compute the lethal events due to the GNP alone ( $D(r)$ ), after subtracting the dose calculated without GNPs in water ( $D(r) = D_{GNP}(r) - D_{water}(r)$ ). The lethal events due to the GNP alone are shown in Equation 4.

$$N_{NP} = \frac{1}{R_C^3} \sum_{r=0}^{R_C} (\alpha D(r) + \beta D(r)^2) ((r + \Delta r)^3 - r^3) \quad (4)$$

Characteristic parameters  $\alpha$  and  $\beta$  were obtained from the experimental cell survival obtained in absence of GNPs. For this study, the lethal events were considered to be inside the nucleus of 9LGS. Therefore  $D(r)$  was calculated from the inside of the GNP shell.

The complete cell survival due to the GNPs ( $S_{NP}$ ) and X-rays was then evaluated with the number of lethal events created by X-ray interaction with the GNP alone ( $N_{NP}$ ) and without the GNP ( $N_X$ ), described in Equation 5.

$$S_{NP} = \exp(-(N_{NP} + N_X)) \quad (5)$$

$S_{NP}$  was evaluated for each dose delivered to water ( $D$  in Eqn. 1), ranging from 1 to 10 Gy. The additional dose predicted by LEM due to the GNPs in  $V_C$  can also be recorded. The effective dose  $D_{eff}$  following treatment with 1 Gy of X-rays in the presence of GNPs was calculated by substituting  $S$  for  $S_{NP}$  in equation 1 and solving for  $D$ . This substitution is shown in equation 6.

$$-\ln(S_{NP}) = \alpha D_{eff} + \beta D_{eff}^2 \quad (6)$$

$D_{eff}$  is the effective dose due to the GNPs and X-rays as calculated by the LEM,  $S_{NP}$  is calculated using equation 5, and the  $\alpha$  and  $\beta$  parameters are due to X-ray irradiation of 9LGS only (no GNPs). The effective dose was calculated using the quadratic formula. The effective dose enhancement  $DE_{eff}$  in  $V_C$  was then derived as  $DE_{eff} = D_{eff} / 1$  Gy. For comparison, the average dose enhancement ( $DE_{av}$ ) in  $V_C$  was also calculated.

### 3. Results

#### 3.1 Experimental Results

To characterize the effect of the AuroVist™ GNPs on 9LGS cells, a clonogenic assay was performed and confirmed that the GNPs did not produce any intrinsic toxicity towards 9LGS cells, with a surviving fraction of  $(1 \pm 0.1)$ . Figure 5 shows the clonogenic surviving fraction of 9LGS cells following irradiation with 150 kVp orthovoltage X-rays with and without GNPs at a nominal concentration of 500  $\mu\text{g}/\text{mL}$ .

The addition of GNPs with increasing X-ray radiation dose, causes radiosensitization of the 9LGS cells, as expected. As a result, the GNPs produce a reduction in the cell surviving fraction (shown by  $S_{NP}$ ) across all doses compared to X-rays

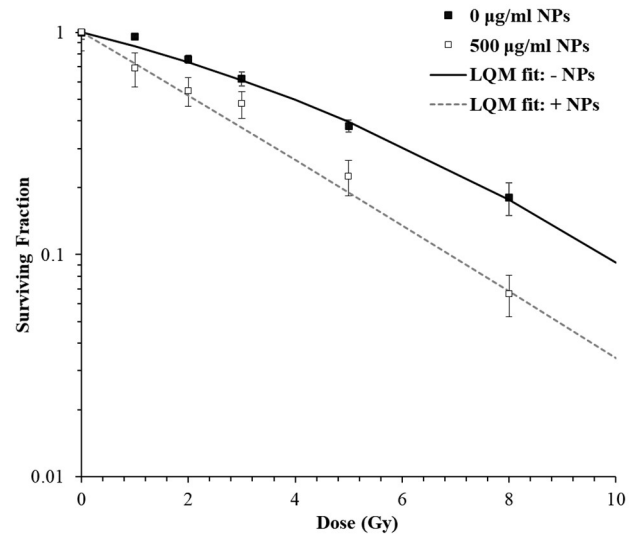


**Figure 5.** Clonogenic surviving fraction of 9LGS following 150 kVp orthovoltage X-ray irradiation, showing the surviving fraction without GNPs, 0  $\mu\text{g}/\text{mL}$  ( $S_X$ ), and with 500  $\mu\text{g}/\text{mL}$  GNPs ( $S_{NP}$ ), and the corresponding linear quadtric model (LQM) fitted lines. The continuous and dashed black lines are the LQM fits to the radiobiological experimental data with without NPs (- NPs) and with (+ NPs), respectively.

alone ( $S_X$ ). The 500  $\mu\text{g}/\text{mL}$  concentration of GNPs and corresponding enhancement is comparable to other radiosensitization studies with kilovoltage X-rays at similar concentrations (McMahon et al. (2011) and Lechtman et al. (2013)). The  $\alpha$  and  $\beta$  parameters, obtained by fitting the SF curves with the LQM model, are shown in Table 1.

Treatment	$\alpha$ ( $\text{Gy}^{-1}$ )	$\beta$ ( $\text{Gy}^{-2}$ )
Control (0 $\mu\text{g}/\text{mL}$ GNPs)	$0.135 \pm 0.052$	$0.011 \pm 0.008$
500 $\mu\text{g}/\text{mL}$ GNPs	$0.334 \pm 0.027$	0

**Table 1.** Summary of the radiobiological parameters ( $\alpha$  and  $\beta$ ) due the radiation treatment of 9LGS cells with (500  $\mu\text{g}/\text{mL}$  GNPs) and without (0  $\mu\text{g}/\text{mL}$ ) GNPs. LQM fits were performed in MATLAB® R2018b using the Curve Fitting Tool™ (MATLAB, 2018). Errors are within a 95% confidence interval.

The primary effect of the addition of GNPs to 9LGS was on the  $\alpha$  parameter, which produces significantly more linearity to the surviving fraction  $S_{NP}$  and is often related to unreparable double strand DNA breaks (McMahon 2019). These parameters will be used in the LEM in the final section.

#### 3.2 Characterization of Physics Models for Gold Nanoparticles in Geant4

##### 3.2.1 Radial dose calculation using different Geant4 physics models

GNP dose enhancement due exposure with an X-ray beam was investigated initially on single GNPs to understand the differences between TS and CH physics models. The radial dose distribution and DER produced around a single GNP of two sizes (7.5 or 50 nm) due to 150 kVp X-rays was compared in Figure 6 using Livermore low energy limit cut (LEE) of 10 eV and G4DNA.

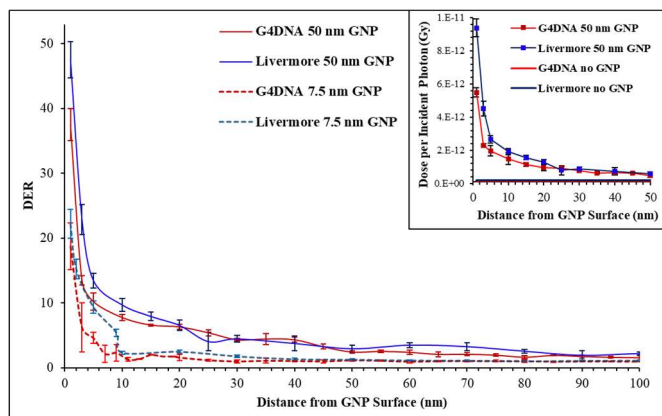


**Figure 6.** Dose enhancement ratio (DER) with respect to the distance from the edge of the GNP, for 7.5 nm and 50 nm radius GNPs, using the specialized TS gold physics models (G4DNA in the legend) and the Livermore models (Livermore in the legend). Inserted graph shows the radial dose per incident photon using each physics model for a 50 nm radius GNP.

CH Livermore physics produced more dose near the GNP than the G4DNA TS models. With a low energy limit of 10 eV (below the recommended 250 eV), the results obtained with Livermore show a DER of  $(22.2 \pm 3.9)$  and  $(47.5 \pm 2.6)$  within 1 nm of the GNP for the 7.5 nm and 50 nm GNP radius, respectively. G4DNA produced DERs of  $(18.7 \pm 3.6)$  and  $(37.5 \pm 1.9)$  at the GNP surface with 7.5 nm and 50 nm GNPs, respectively, due to an overall greater electron stopping power in gold with the TS approach, as noted by Sakata *et al.* (2018). DER decreases with distance as low-energy secondary electrons originating in the GNP deposit energy locally in the surrounding biological medium. Sakata *et al.* (2018) likewise shows additional absorbed dose produced with Livermore (but with LEE=250 eV) compared to TS models up to 1  $\mu\text{m}$  from the center of a GNP with radius 30 nm.

The DER becomes equal to 1 at a radial distance of 250 nm using the 50 nm radius GNP for both TS and Livermore models in our case. After this, the statistical fluctuation of DER lies within 3% of 1 (equivalent to water) within 95% confidence level. However, some secondary electrons created by the GNP can travel to micrometer distances away from the GNP, but these do not produce a significant change to the DER produced by a single GNP.

### 3.2.2 Effect of Auger electrons on the radial dose distribution

The Auger electrons are suspected to be responsible for significant dose enhancement near GNPs (McMahon *et al* 2011). Auger generation was switched off in the GNP region only and compared to complete Auger activation throughout all volumes between Livermore (LEE=10 eV) and G4DNA models in Figure 7.

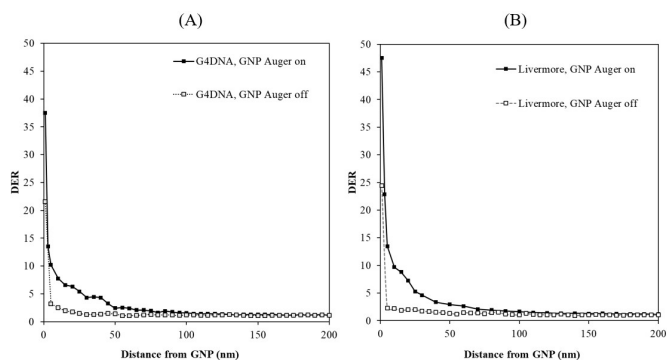


**Figure 7.** A comparison of the effect on the DER due to Auger electrons produced by the GNP using G4DNA (A) and Livermore physics models (LEE=10 eV) (B). For each physics model, Auger electron production in the GNP was switched off (white boxes) and compared with the case with GNP Auger electrons switched on (black boxes).

Our results confirm that Auger electrons have a significant impact on the energy deposited near the GNP, as noted in previous studies (McMahon *et al* 2011). The additional dose produced by the Auger electrons emitted by the 50 nm GNP is  $(43. \pm 1.)\%$  and  $(53. \pm 2.) \%$  when considering distances up to 500 nm from the GNP surface, using the G4DNA and Livermore physics models (LEE=10 eV), respectively.

### 3.2.3 Effect of the low electron energy limit cut

The kinetic energy of the secondary electrons leaving the GNP was scored for both the Livermore approach and the G4DNA models to compare the effect of changing the Livermore LEE with G4DNA. Figure 8 shows the kinetic energy spectra and number of electrons per incident photon emerging from a 50 nm radius GNP.

The spectra calculated with the two physics approaches are similar for energies above  $\sim 1$  keV. For lower energies Livermore tends to produce more electrons, on average  $(1.4 \pm 0.3)$  times for electrons below 5 keV, which is expected due to the higher stopping power of the G4DNA models for gold and accurate modelling of the production and transport of low energy electrons (Sakata *et al* 2018). Overall, G4DNA produces fewer electrons from the GNP than Livermore.

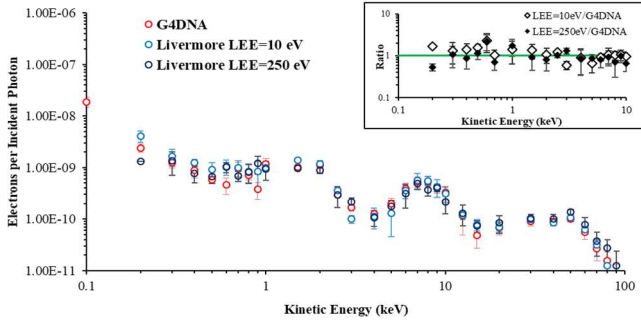


**Figure 8.** Kinetic energy spectra of electrons leaving the GNP using G4DNA and Livermore physics models (LEE = 10 eV and LEE = 250 eV). The main plot shows the kinetic energy of electrons per incident photon for G4DNA (red), Livermore LEE = 10 eV (light blue) and LEE = 250 eV (dark blue). The inserted graph shows the ratio of the number of electrons emitted when activating Livermore and G4DNA. Minimum bin size is 0.1 keV.

The Livermore LEE = 250 eV spectra shows that there are no electrons with energy below 250 eV, as expected. The LEE of 250 eV results in more energy deposition near the GNP due to the lost energy being deposited locally rather than converted into  $\delta$ -electrons.

The average kinetic energy of electrons emerging from the GNP is  $(18 \pm 1)$  keV,  $(21 \pm 1)$  keV and  $(24 \pm 1)$  keV, when using the G4DNA and Livermore LEE = 10 eV and 250 eV, respectively. These energies correspond to ranges between 7  $\mu\text{m}$  to 9.5  $\mu\text{m}$  in water, and 1  $\mu\text{m}$  and 1.45  $\mu\text{m}$  in gold (Berger et al 2000). Therefore, the average electron will traverse a single GNP without self-absorption for both 7.5 nm and 50 nm radius GNPs.

Figure 9 shows the effect of changing the Livermore LEE from 10 eV to 250 eV in terms of radial dose distribution and DER, in the case of a GNP with a 50 nm diameter.

10 eV LEE provides a much better agreement with G4DNA than the 250 eV limit, confirming the results of Lazarakis *et al* (2013) and Kyriakou *et al* (2019). When using LEE=250 eV, Livermore produces larger doses that diverges from G4DNA by 37% within 10 nm from the GNP surface. The LEE=250 eV Livermore produces a large dose deposition near the GNP due to the higher electron production cut leading to a higher local energy deposition. These results show that the Livermore physics models, with a LEE of 10 eV, could be used when calculating the dose at sub- $\mu\text{m}$  scale if TS codes are not available. This should be done with care, given that the authors of the Livermore models recommend its use down to 250 eV.

Thus far, differences between G4DNA with TS-based code and CH Livermore have been identified for GNP simulations involving radial dose on the nanoscale in a kV field. The next section will compare models for more ‘realistic’ GNP geometry which will be used for the LEM comparison.

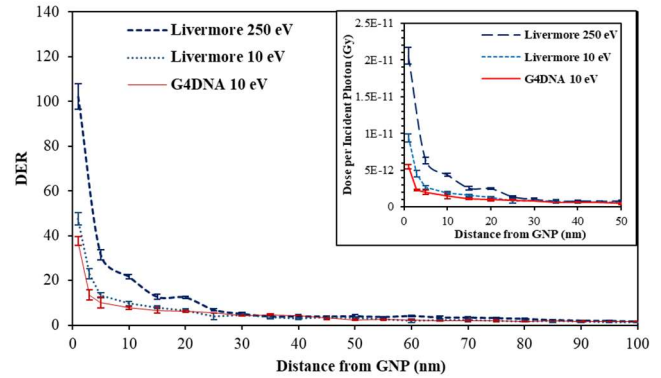


**Figure 9.** Radial dose distribution obtained with LEE equal to 10 eV and to 250 eV in the case of the Livermore physics. DER is shown on main plot and radial dose per incident photon on inserted graph.

### 3.3 Partial shell GNP configuration and in silico cell survival

Rarely GNPs accumulate homogeneously within cells, instead GNPs aggregate into new configurations, such as the “shell”-like structures in 9LGS (see Figure 1). We simulated the shell to be 1 GNP (15 nm) thick based on confocal imaging and constructed to surround 60% of the 9LGS nucleus volume with radius 5  $\mu\text{m}$ , shown in the insert on Figure 10. The entire radial dose on the nanoscale was recorded inside  $V_C$ , in Figure 10, and extending 1  $\mu\text{m}$  beyond.

The dose per incident photon between Livermore and G4DNA is significantly different both in water and when the GNP shell is present. Livermore produces  $(30 \pm 4)\%$  more dose than G4DNA in water alone. Using the data presented in Figure 10, Figure 11 shows the resulting radial DER for each physics model due to the GNP shell, including an insert showing more detail within 200 nm of the GNP surface. In this case the significant dose discrepancy between Livermore and G4DNA is eliminated by normalizing to water in the DER calculation. However, there is still significant differences in the absorbed dose near the GNP.

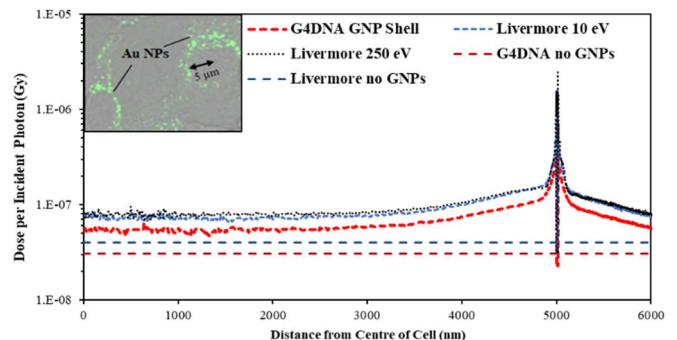


**Figure 10.** Dose per incident photon due to the GNP shell with Livermore LEE=10 eV (blue) and LEE = 250 eV (black), compared to G4DNA (red). The inserted image shows a 9LGS cell including the radius of the cell nucleus.

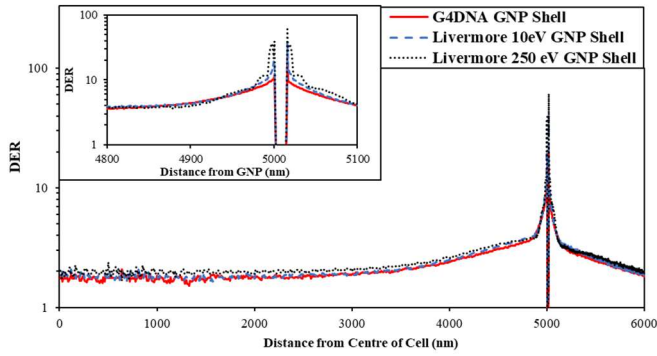


**Figure 11.** ‘Realistic’ GNP distribution radial DER using G4DNA (red) and Livermore physics with a 10 eV (blue) and 250 eV LEE (black). The DER near the GNP shell is zoomed in the top insert.

The DER inside  $V_C$  never approaches 1 in contrast to the case of a single GNP where  $DER=1$  from  $\sim 70$  nm from the edge of the nanoparticle. This occurs due to the greater number of high energy electrons that have been produced from the greater likelihood of X-ray interaction with gold (the shell is made of thousands of single GNPs). This highlights the benefit of the GNP-shell formation in largely increasing the dose to the nucleus of cancer cells without having to be internalized into the nucleus, as mentioned in previous studies as an ideal case to produce Auger electrons near DNA (Engels et al 2017, McKinnon et al 2016).

Comparing directly between CH Livermore with LEE=10 eV and LEE=250 eV and G4DNA for the GNP shell, Livermore consistently produces greater radial dose and DER near the GNP surface, as noted in the previous section. The Livermore (LEE=10 eV) DER converges to the G4DNA DER after 800 nm from the GNP surface, whereas the LEE =250 eV never completely converges to G4DNA.

### 3.4 Evaluating LEM-based radiobiological models for clustered shell GNP configurations

The expected surviving fraction of 9LGS with GNPs ( $S_{NP}$ ) using the LEM was calculated from the radial dose profiles presented in Figure 10 and Figure 11, for CH Livermore (LEE=10eV and LEE=250eV) and G4DNA TS codes. The resulting  $S_{NP}$  for the models is shown in Figure 12, compared to the experimental data for  $S_{NP}$  and  $S_X$  (no GNPs).

Using the ‘realistic’ GNP distribution, the LEM method agrees with the experimental results. The large changes in the DER gradient from the surface of the GNP shell are evaluated through calculation of the lethal events at each 1 nm step from the shell using LEM.

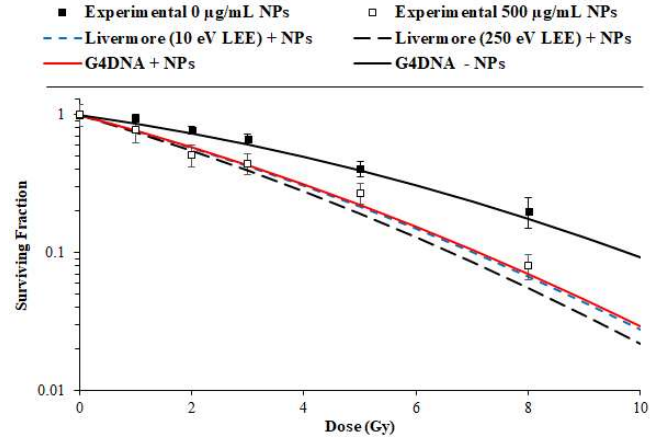


**Figure 12.** Predicted cell surviving fraction using the LEM for the ‘realistic’ GNP shell distribution modelled with G4DNA (red line), Livermore physics with LEE = 10 eV (blue line) and LEE = 250 eV (black line). The LEM-computed survival without GNPs is shown for G4DNA. Experimental data with ( $S_{NP}$ ) and without ( $S_X$ ) GNPs, (white and black squares, respectively) is overlaid. In the legends, “+ NP” and “-NP” indicate with and without the NP in the biological medium.

This allows an effective dose due to the inhomogeneous dose field of the GNPs to be calculated inside  $V_C$ .

Table 2 shows a comparison of the effective dose enhancement due to the GNP shell in  $V_C$  using the LEM ( $DE_{eff}$ ) as calculated using Equation 6, with the average dose enhancement in  $V_C$  ( $DE_{av}$ ) for each of the physics models considered.

	G4DNA	Livermore LEE 10 eV	Livermore LEE 250 eV
$DE_{eff}$	1.72	1.75	1.89
$DE_{av}$	$2.22 \pm 0.03$	$2.28 \pm 0.03$	$2.44 \pm 0.04$

**Table 2.** Effective dose enhancement in  $V_C$  using LEM, compared to the average DER in  $V_C$ , determined using G4DNA and Livermore physics with LEE= 10 eV and 250 eV.

The  $DE_{eff}$  is smaller than the average dose enhancement in  $V_C$  for each physics approach considered. This is due to the calculation of the cell survival with GNPs at each radial dose step from the GNP shell minimizing the impact of the large dose near the GNP shell. In contrast,  $DE_{av}$  is affected by this initial large radial dose near the GNP surface (as seen in Figure 11). This is a result of the assumption that there is no interaction between GNP-related dose and water-only related dose (Equation 5), which reduces the impact of the added dose from the NPs. As a result, the average dose enhancement provides over 2.2 times the dose in water alone for each physics model and would cause a significant divergence in the predicted LQM cell survival. For this study, the  $DE_{av}$  was therefore not appropriate for GNP modelling of cell survival with our GNP distribution.

Instead, the similar  $DE_{eff}$  produced by G4DNA and 10 eV LEE Livermore produced a good agreement with the experimental data. The higher effective dose enhancement using the 250 eV LEE Livermore model increased the predicted cell killing of the  $S_{NP}$ , as seen in Figure 12.

#### 4. Discussion

This study has characterized the variations in absorbed dose to water produced by single GNPs in an X-ray field due to TS and CH physics models in Geant4. We applied these findings to simplistically model a GNP distribution in Geant4 confocal imaging of GNPs in 9LGS cells, and calculate the corresponding cell survival using the LEM. Our results show that the new TS-based G4DNA models for gold can produce a good correlation to experimental GNP radiosensitization, if considering the nanoscale dose and a partial-shell GNP structure.

Livermore CH models with an LEE of 10 eV provided a dose enhancement result that was more consistent with the TS model than when using the recommended LEE of 250 eV.

Livermore physics produced 30% more dose in water than G4DNA. The greatest difference between G4DNA and Livermore was the larger DER at the GNP surface regardless GNP size, and further increased when increasing the cut threshold from 10 eV to 250 eV.

Livermore at LEE = 10 eV overall produced good agreement to G4DNA, in agreement with Lazarakis *et al.* (2018) and Kyriakou *et al.* (2019). However, Livermore is not recommended to be used below 250 eV, (Cullen *et al.* 1991, 1997, Perkins *et al.* 1991) with significant differences in terms of spectra of low energy secondary electrons and calculation of energy deposition around GNPs with respect to G4DNA (Sakata *et al.* 2016, 2018).

When using TS and CH models, Auger electrons are predominantly contributing to single GNP dose enhancement. For small radii, this happens when the GNPs are situated near or inside the cell nucleus to maximize the DNA damage. With larger GNP distributions, where multiple GNPs interact to enhance the dose to the cell, the higher energy electrons, and not the Auger electrons, enhance significantly the dose distribution over micrometer distances (McKinnon *et al.* 2016, Coulter *et al.* 2002).

Previous studies have scarcely considered the effect of a more realistic GNP distribution in the LEM when translating Monte Carlo results to radiobiological experiments. Instead, single GNPs are often used (Ferrero *et al.* 2017, McMahon *et al.* 2011) with one study randomizing GNP positions within the cell before applying the LEM using PENELOPE CH models (Lechtman *et al.* 2013).

The distribution of GNPs must be considered carefully as it is known to differ between cell lines (McMahon *et al.* 2011, Brown and Currel 2017). More homogeneously distributed GNPs in cells can produce good agreement between using a

single GNP and the LEM, as the GNP systems are more isolated and significant dose enhancements occur within 10-100 nm. However, in some cell lines (such as 9LGS), the clustering of NPs causes superimposing and shielding effects on the dose enhancement (McKinnon *et al.* 2016). Brown and Currel (2017) include components accounting for dose saturation when NP shells form around 9LGS, and other cell lines in the LEM calculation. In our study, electrons with energies between 10-100 keV (Figure 8) have a larger role in the dose enhancement in the cell when the GNPs are configured in a “shell-like” distribution. This was also noted by McKinnon *et al.* (2016) and in other kV applications with NPs (Engels *et al.* 2016). Our GNP layer around 9LGS cells can be thicker than 1 GNP realistically (see Figure 1) and can be partially incomplete around the cell nucleus. This in turn affects the dose to the nucleus and nearby cells, and may be of interest in future simulations.

Modelling multiple GNPs with accurate physics models and including real GNP distributions is an important step to advance the modelling of NP radioenhancement by means of the LEM and Monte Carlo simulations. Future studies should also consider the effect of indirect radiation damage by modelling radiochemistry (Bernal *et al.* 2015) and other radiobiological models besides LEM which incorporate DNA damage on the nanoscale (Garty *et al.* 2010).

#### 5. Conclusion

This research marks the first use of the new Geant4 TS-based models for gold to predict GNP dose enhancement in a cancerous cell line. This study has investigated simulation physics models (CH and TS) and parameters (LEE) to describe GNP radioenhancement in kV beam when considering a distribution of GNPs that more resembles the configuration of GNPs seen in an *in vitro* cell population.

We have demonstrated a noticeable difference in physics models in Geant4 on the nanoscale dose around a gold nanoparticle. Overall, (CH) Livermore physics overestimated the dose and dose enhancement with GNPs compared to Geant4-DNA models. The advantage of the TS-models in this study was an accurate secondary electron production and tracking, which led to significant differences in terms of dose calculation to the Livermore close to the GNP surface. Accurate low-energy electron tracking will become more important for further studies investigating GNP radioenhancement considering realistic distributions of the gold nanoparticles and when including the chemical stage modelling (radiolysis). When the TS models are not available for modelling NP dose, using Livermore with a 10 eV LEE appears to be an alternative for NP dose calculations. In addition, we underlined the necessity of simulating fully Auger emission, which directly impacts DER.

The Local Effect Model (LEM) was used to calculate the cancer cell survival according to an approximation of a more

realistic GNP distribution. A good agreement was found between the simulation results and the experimental measurements. To our knowledge, this is the first study to use a shell-like geometric model of GNPs in the translation of Monte Carlo to experimental data with the LEM. In future, simulations should consider more realistic conditions, and we will be considering an alternative model which instead calculates the direct and indirect (chemical) damage of radiation in a GNP configuration that is based in individual particle positions in the cell.

This work contributes to the translation of Monte Carlo based studies in GNP dose enhancement to experimental GNP radiosensitization. This study highlights the benefits of combining state of the art Monte Carlo simulation with biological imaging, radiobiological models and *in vitro* studies.

## Acknowledgements

We would like to acknowledge the University of Wollongong (UOW) Information Technology Services (ITS), the Centre for Medical Radiation Physics, and the Australian National Computational Infrastructure (NCI) for computing time and resources. We acknowledge the access facilities at the Illawarra Health and Medical Research Institute, and Prince of Wales Hospital, Randwick, NSW, Australia. We acknowledge the financial support of the Australian Government Research Training Program Scholarship, Australian Research Council (DP170100967) and Australian National Health & Medical Research Council (APP1084994).

## References

- [1] Jain S, Hirst DG, and O’Sullivan JM 2012 *The British Journal of Radiology*, **85**, 101–113.
- [2] Engels E, Lerch M, Tehei M, Konstantinov K, Guatelli S, Rosenfeld AB, and Corde S 2017 *Journal of Physics: Conference Series*, **777**, 1.
- [3] Engels E, Westlake M, Li N, Vogel, S, Gobert Q, Thorpe N, Rosenfeld AB, Lerch MLF, Corde S, Tehei M 2018 *Biomedical Physics & Engineering Express*, **4**, 4.
- [4] Chithrani BD, Stewart J, Allen C, Jaffray DA 2009 *Nanomedicine: Nanotechnology, Biology, and Medicine*, **5**, 2, 118–127.
- [5] Her S, Jaffray DA, Allen C 2017 *Advanced Drug Delivery Reviews*, **109**, 84–101.
- [6] Tran HN, Karamitros M, Ivanchenko VN, Guatelli S, McKinnon S, Murakami K, Sasaki T, Okada S, Bordage MC, Francis, Z. *et al.* 2016 *Nuclear Instruments and Methods in Physics Research, Section B: Beam Interactions with Materials and Atoms*, **373**, 126–139.
- [7] McKinnon S, Engels E, Tehei M, Konstantinov K, Corde S, Oktaria S, Incerti S, Lerch M, Rosenfeld AB, Guatelli S 2016 *Physica Medica*, **32**, 10, 1216–1224.
- [8] Liu, R, Zhao, T, Zhao, X, Reynoso, FJ 2019 *Medical Physics*, **46**, 5314–5325
- [9] Zygmanski P and Sajo E 2016 *British Journal of Radiology*, **89**, 20150200.
- [10] McDonald M, Oktaria S, Konstantinov K, Rosenfeld AB, Lerch M, Corde S, Tehei M 2018 *Biomedical Physics & Engineering Express* **4**, 3.
- [11] Lin Y, McMahon SJ, Scarpelli M, Paganetti H, Schuemann J 2014 *Physics in Medicine & Biology*, **59**, 7675.
- [12] Hainfeld JF, Dilmanian FA, Slatkin DN, Smilowitz HM 2008 *Journal of Pharmacy and Pharmacology*, **60**, 977–985.
- [13] Hainfeld JF, Smilowitz HM, O’Connor MJ, Dilmanian FA, Slatkin DN 2013 *Nanomedicine (Lond)*, **8**, 10, 1601–1609.
- [14] Mesbahi A 2010 *Reports of Practical Oncology and Radiotherapy*, **15**, 176–180.
- [15] Kim SR, and Kim EH 2017 *International Journal of Radiation Biology* **93**, 5, 517–526
- [16] Kim SR, and Kim EH 2018 *International Journal of Radiation Biology*, **94**, 1, 8–16.
- [17] Grotzer MA, Schültke E, Bräuer-Krisch E, Laissue JA 2015 *Physica Medica*, **31**, 564e567
- [18] Joh DY, Sun L, Stangl M, Al Zaki A, Murty S, Santoiemma PP, Davis JJ, Baumann BC, Alonso-Basanta M, Bhang D *et al.* 2013 *PLoS ONE*, **8**, 4, e62425
- [19] Engels, E., Li, N., Davis, J. *et al.* 2020 Toward personalized synchrotron microbeam radiation therapy. *Sci Rep* **10**, 8833.
- [20] Boudou C, Balosso J, Esteve F, Elleaume H 2005 *Physics in medicine and biology*, **50**, 20, 4841.
- [21] Jones BL, Krishnan S, Cho SH 2010 *Medical Physics* **37**, 3809–3816.
- [22] Cho SH 2005 *Physics in Medicine & Biology*, **50**, 15, N163.
- [23] Nelson WR, Hirayama H, Rogers DWO The EGS4 CODE SYSTEM; Technical report SLAC-265; Stanford Linear Accelerator Center Stanford University: Stanford, CA, USA, 1985.
- [24] Baró J, Sempau J, Fernández-Varea JM, Salvat F, 1995 *Nuclear Instruments and Methods in Physics Research Section B: Beam Interactions with Materials and Atoms*, **100**, 1, 31–46.
- [25] Agostinelli S, Allison J, Amako K, Apostolakis J, Araujo H, Arce P, Asai M, Axen D, Banerjee S, Barrand G. *et al.* 2003 *Nuclear Instruments and Methods in Physics Research Section A*, **506**, 250–303.
- [26] X-5 Monte Carlo Team. MCNP—A General Monte Carlo N-Particle Transport Code, Version 5 (1-2). Los Alamos National Laboratory, Los Alamos, 2005.
- [27] Grosswendt B 2002 *Radiation and Environmental Biophysics*, **41**, 2, 103–12.
- [28] Friedland W, Dingfelder M, Kunderát P, Jacob P. 2011 *Mutat Res.* 711(1-2), 28–40.
- [29] Nikjoo H, Emfietzoglou D, Liamsuwan T, Taleei R, Liljequist D, Uehara S 2016 *Reports on Progress in Physics* **79**, 116601–55.
- [30] Semenenko VA, Turner JE, Borak TB 2003 *Radiation and Environmental Biophysics*, **42**, 3, 213–7.
- [31] Arce P. *et al.* 2020 *Medical Physics*, accepted for publication on the 11<sup>th</sup> May 2020, in press.
- [32] Cirrone PGA, Cuttone G, Di Rosa F, Pandola L, Romano F, Zhang Q 2010 *Nuclear Instruments and Methods in Physics Research Section A Accelerators Spectrometers Detectors and Associated Equipment*, **618**, 315–322.
- [33] Cullen DE, Hubbell JH, Kissel L 1997 *Report UCRL-50400*, vol. 6.

- [34] Cullen DE, Perkins ST, Seltzer SM 1991 *UCRL-50400*, vol. **31**.
- [35] Perkins ST, Cullen D, Chen MH, Rathkopf J, Scofield J, Hubbell JH 1991 *UCRL-50400*, vol 30.
- [36] Fernandez-Varea JM, Gonzalez-Munoz G, Galassi ME, Wiklund K, Lind BK, Ahnesjo A, Tilly N 2012 *International Journal of Radiation Biology* **88**, 66–70.
- [37] Lazarakis P, Incerti S, Ivanchenko V, Kyriakou I, Emfietzoglou D, Corde S, Rosenfeld AB, Lerch M, Tehei M, Guatelli S 2018 *Biomedical Physics & Engineering Express*, **4** 024001
- [38] Kyriakou I, Ivanchenko V, Sakata D, Bordage MC, Guatelli S, Incerti S, Emfietzoglou D 2019 *Physica Medica*, **58**, 149-154.
- [39] Incerti S, Ivanchenko A, Karamitros M, Mantero A, Moretto P, Tran HN, Mascialino B, Champion C, Ivanchenko VN, Bernal MA 2010 *Medical Physics*, **37**, 4692-4708.
- [40] Incerti S, Baldacchino G, Bernal M, Capra R, Champion C, Francis Z, Guèye P, Mantero A, Mascialino B, Moretto P *et al.* 2010 *International Journal of Modeling, Simulation, and Scientific Computing* **1**, 2, 157-178.
- [41] Bernal MA, Bordage MC, Brown JMC, Davidková M, Delage E, El Bitar Z, Enger SA, Francis Z, Guatelli S, Ivanchenko VN *et al.* 2015 *Physica Medica*, **31**, 861-874.
- [42] Incerti S, Kyriakou I, Bernal MA, Bordage MC, Francis Z, Guatelli S, Ivanchenko V, Karamitros M, Lampe N, Lee SB *et al.* 2018 *Medical Physics*, **45**, 8, e722-739.
- [43] Sakata D, Incerti S, Bordage MC, Lampe N, Okada S, Emfietzoglou D, Kyriakou I, Murakami K, Sasaki T, Tran H. *et al.* 2016 *Journal of Applied Physics* **120**, 24, 244901-1-244901-7.
- [44] Sakata D, Kyriakou I, Okada S, Tran HN, Lampe N, Guatelli S, Bordage MC, Ivanchenko V, Murakami K Sasaki T. *et al.* 2018 *Medical Physics*, **45**, 5, 2230-2242.
- [45] Sakata D, Kyriakou I, Tran KH, Bordage M, Rosenfeld AB, Ivanchenko V, Incerti S, Emfietzoglou D, Guatelli S 2019 *Physica Medica*, **63**, 98-104.
- [46] McMahon SJ 2019 *Physics in Medicine & Biology* , **64**, 1.
- [47] Lechtman E, Mashouf S, Chattopadhyay N, Keller BM, Lai P, Cai Z, Reilly RM, Pignol JP 2013 *Physics in Medicine and Biology*, **58**, 3075–3087.
- [48] Scholz M, Kraft G. 1994 *Radiation Protection Dosimetry*, **52**, 29–33.
- [49] Scholz M, Kraft G 1996 *Advances in Space Research*, **18**, 5-14.
- [50] Scholz M, Kraft G 2004 *Radiation Research*, **161**, 612-620.
- [51] Ferrero V, Visonà G, Dalmasso F, Gobbato A, Cerello P, Strigari L, Visentin S, Attili A 2017 *Medical Physics*, **44** (5).
- [52] McMahon SJ, Hyland WB, Muir MF, Coulter J, Jain S, Butterworth KT, Schettino G, Dickson GR, Hounsell A, O'Sullivan JM *et al.* 2011 *Scientific Reports*, **1**.
- [53] McQuaid HN, Muir MF, Taggart LE, McMahon SJ, Coulter JA, Hyland WB, Jain S, Butterworth KT, Schettino G, Prise KM *et al* 2016 *Scientific Reports*, **6**, 19442.
- [54] Bobyk L, Edouard M, Deman P, Vautrin M, Pernet-Gallay K, Delaroche J, Adam JF, Estève F, Ravanat JL Elleaume H 2013 *Nanomedicine*, **9**,1089-1097.
- [55] Domey J, Teichgräber U, Hilger I 2015 *International Journal of Nanomedicine*, **10**, 3803–3814.
- [56] Kim CS, Li X, Jiang Y, Yan B, Tonga GY, Ray M, Solfield DJ, Rotello VM 2015 *MethodsX*, **2**, 306–315.
- [57] Poludniowski G, Landry G, DeBlois F, Evans PM, Verhaegen, F 2009 *Physics in Medicine and Biology*, **54**,19, N433-8.
- [58] Guatelli S, Mantero A, Mascialino B, Nieminen P, Grazia Pia M 2007 *IEEE Transactions on Nuclear Science*, **54**,3, 585-593.
- [59] MATLAB, 2018. version 9.5 (R2018b), Natick, Massachusetts: The MathWorks Inc.
- [60] Berger MJ, Coursey JS, Zucker MA 2000 MD, Gaithersburg: National Institute of Standards and Technology.
- [61] Coulter JA, Jain S, Butterworth KT 2002 *International Journal of Nanomedicine*, **7**, 2673–2685.
- [62] Brown JMC, Currell FJ 2017 *Cancer Nanotechnology*, **8**,1,1.
- [63] Engels E, Corde S, McKinnon S, Incerti S, Konstantinov K, Rosenfeld AB, Tehei M, Lerch MLF, Guatelli S 2016 *Physica Medica*, **32**,12, 1852-1861.
- [64] Garty G; Schulte R, Shchemelinin S, Leloup C, Assaf G, Breskin A, Chechik R, Bashkirov V, Milligan J, Grosswendt B 2010 *Physics in Medicine & Biology*, **55**, 3,761-81.